Supporting Information for "Contrasting Nighttime Heterogeneous and Daytime Photochemical Aging Drive the Optical Evolution of Black Carbon"

Yin Zhang[1,2], Jinghao Zhai[1,3], Yaling Zeng[1,2], Shao Shi[1,2], Baohua Cai[1,2], Ke Yang[1,2], Yu Yan[1,2], Xin Yuan[1,2], Tianlong Hu[1,2], Chen Wang[1,2], Tzung-May Fu[1,2], Lei Zhu[1,2], Huizhong Shen[1,2], Jianhuai Ye[1,2], and Xin Yang[1,2]

[1]Shenzhen Key Laboratory of Precision Measurement and Early Warning Technology for Urban Environmental Health Risks, School of Environmental Science and Engineering, Southern University of Science and Technology, Shenzhen 518055, China
[2]Guangdong Provincial Field Observation and Research Station for Coastal Atmosphere and Climate of the Greater Bay Area, Southern University of Science and Technology, Shenzhen, Guangdong, 518055, China
[3]Department of Geophysical Sciences, University of Chicago, Chicago 60637, IL, United States

Correspondence: Jinghao Zhai (jinghao@uchicago.edu) and Xin Yang (yangx@sustech.edu.cn)

1 PMF analysis

Positive matrix factorization (PMF), a widely used multivariate receptor model, operates under the assumption that chemical species exhibiting similar temporal trends likely originate from common sources. Owing to this principle, PMF has been extensively applied in aerosol source apportionment studies, particularly for resolving the mass contributions of individual components (Polissar et al., 1998; Reff et al., 2007).

Beyond mass concentration analysis, PMF has also proven effective in processing particle-type data obtained from mass spectrometry, offering valuable insights into emission characteristics and secondary transformation processes (Healy et al., 2015; Zhang et al., 2021). In the present study, we applied the U.S. EPA PMF 5.0 model to classify BC-containing particles based on their chemical signatures. Specifically, 11 ion markers from all detected EC particles were grouped using 60-minute averaged relative peak areas (RPAs) as input. It is worth noting that our application of PMF was not aimed at identifying distinct emission sources; instead, the goal was to cluster chemically similar markers for further interpretation.

Solutions with 2–6 factors were tested, and the results are summarized in TableS1. Across all solutions, Q_{robust} was slightly lower than Q_{true}. The 4-factor solution was ultimately selected because it exhibited high correlations between measured and predicted species concentrations ($R^2 = 0.42$–0.96) and because the factors were the most physically interpretable. The residuals for this solution ranged from -3 to 3. F_{peak} values ranging from -1.5 to 1.5 were evaluated, and analysis of the Q values indicated that an F_{peak} of 0 provided the optimal results.

Table S1. Q values for PMF analysis with different number of factors.

# of factors	R^2 between observed and predicted species	Q_{true}	Q_{robust}
2	0.35–0.80	17173.9	13402.1
3	0.37–0.93	9657.3	8638.5
4	0.42–0.96	7061.8	6538.2
5	0.44–0.96	5344.1	4927.0
6	0.56–0.98	3521.1	3431.6

2 Adjustment of the rBC MAC

Given that some BrC is known to absorb at 532 nm(Zhai et al., 2025) and measurements at longer wavelengths were unavailable, we adopted the method proposed by Cappa et al. (2019) to isolate the BrC contribution from the total absorption. By determining the MR-dependent absorption enhancement (Fig. S8a), the mixing-induced absorption enhancement at different MR can be quantified. Subsequently, the absorption contribution of BrC can be derived from the difference between the measured total absorption and the estimated absorption of the coated BC:

$$b_{\mathrm{abs,BrC}} = b_{\mathrm{abs,obs}} - b_{\mathrm{abs,BC,coated}} = b_{\mathrm{abs,obs}} - \mathrm{MAC}_{\mathrm{BC,ref}} \cdot E_{\mathrm{abs}}(MR) \cdot [\mathrm{rBC}] \tag{1}$$

where $b_{\mathrm{abs,BrC}}$, $b_{\mathrm{abs,obs}}$, and $b_{\mathrm{abs,BC,coated}}$ are the absorption by BrC, the observed absorption, and the estimated absorption for coated BC particles, respectively. The MAC of rBC was further corrected by subtracting $b_{\mathrm{abs,BrC}}$. This adjustment only accounts for the significant daytime BrC contribution to the total absorption, which is attributed to low rBC loadings and enhanced BrC absorption. In contrast, because high rBC concentrations dominate the optical absorption at night and yield physically meaningless negative $b_{\mathrm{abs,BrC}}$ values (Fig S8b), the BrC contribution is deemed negligible, and this correction is thus bypassed for nighttime periods.

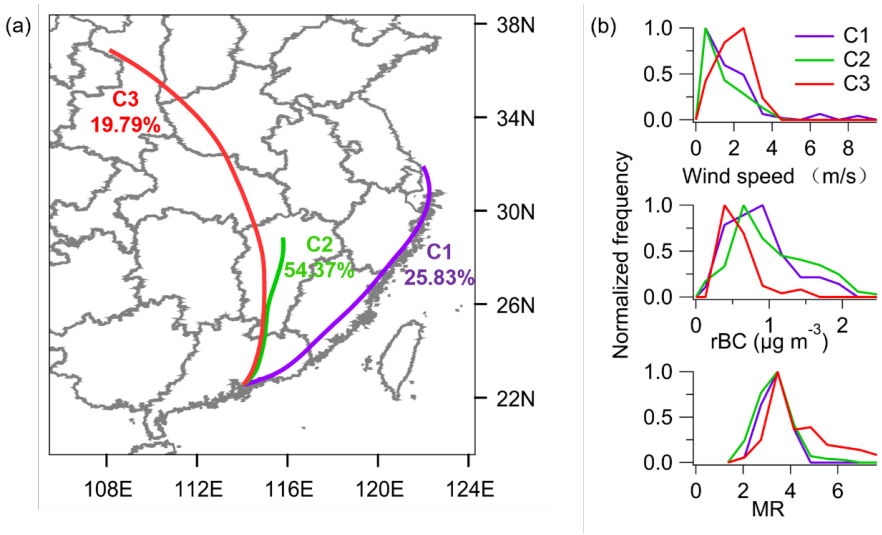

Figure S1. (a) The HYSPLIT 72-hr backward trajectory clusters ending in Shenzhen at 00:00 local time on 9 December 2021, from a height of 100 m. (b) Histograms of wind speed, rBC mass concentration and mixing ratio (MR) for each classified air mass category.

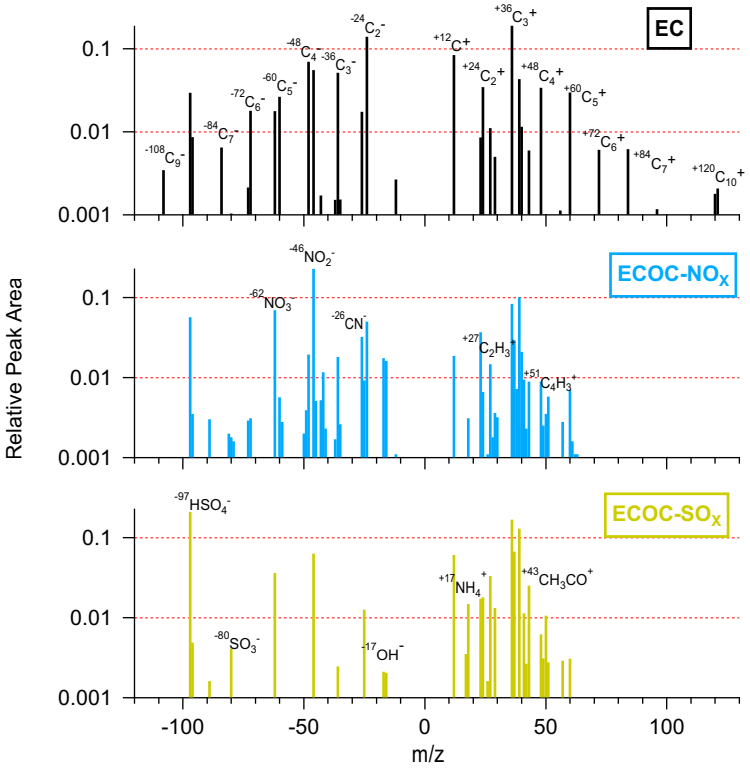

Figure S2. Averaged mass spectra for different BC-containing types of particles.

The cluster-averaged mass spectra of individual BC-containing particles are shown in Fig. S2. The EC group exhibits strong signals for elemental carbon (C_n^- and C_n^+), accompanied by relatively high signals for organic carbon (*m/z* 27 [$C_2H_3^+$] and *m/z* 29 [$C_2H_2^+$]). The ECOC-NO_x and ECOC-SO_x groups exhibit similar mass spectral patterns in terms of chemical composition, with more ion peaks than the EC group. The primary distinction between them lies in the relative intensities of the sulfate (*m/z* -97 [HSO_4^-]) and nitrate (*m/z* -46 [NO_2^-] and *m/z* -62 [NO_3^-]) signals.

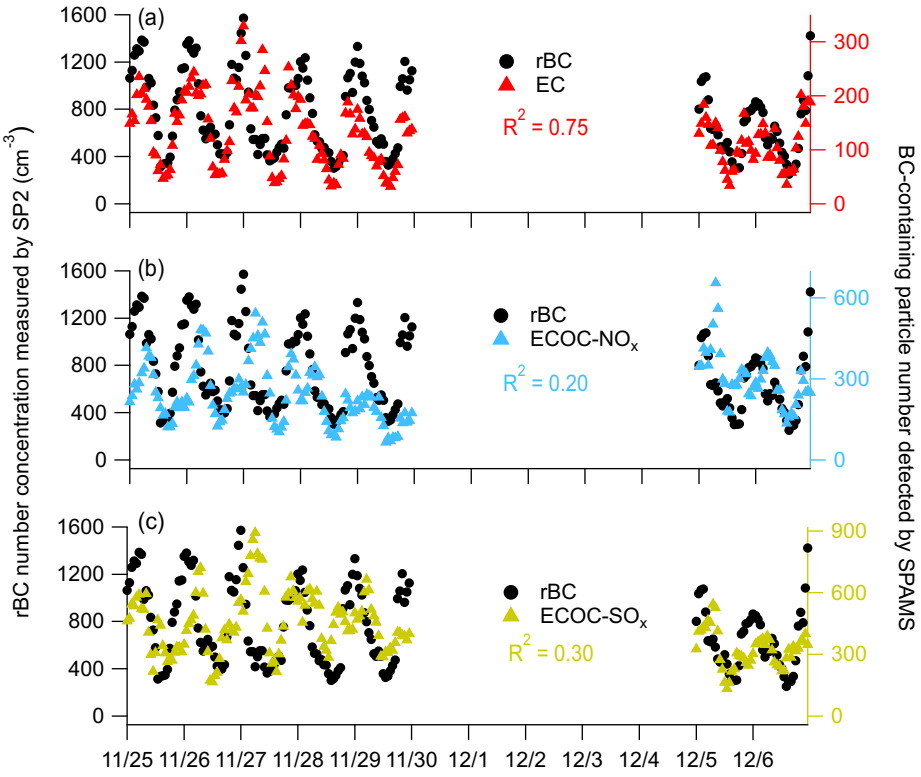

Figure S3. The comparison of SP2-detected rBC number concentration and SPAMS-detected BC containing particle number.

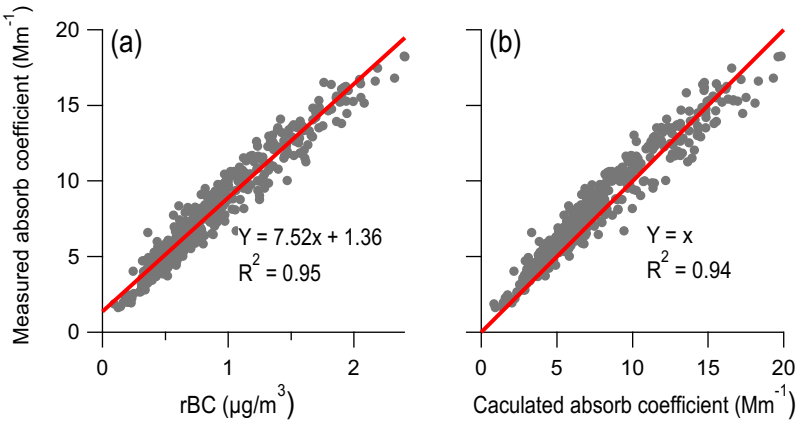

Figure S4. Relationships between the absorption coefficient measured by PAX and (a) the rBC mass concentration, and (b) the absorption coefficient calculated from SP2-measured D_c and D_p using the core-shell Mie model.

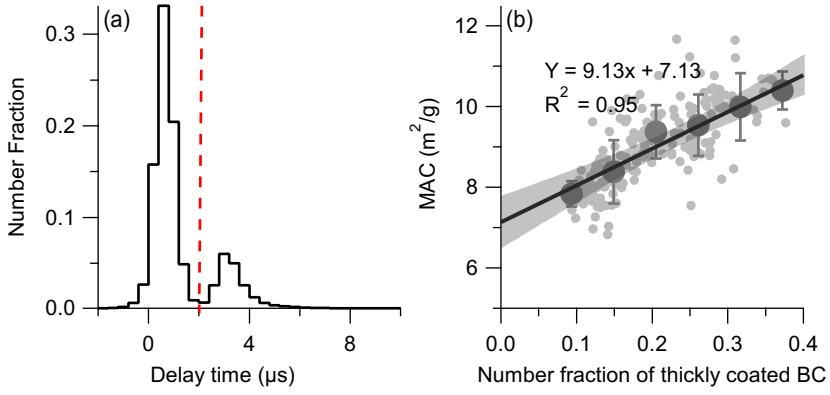

Figure S5. (a) Frequency distribution of the time lag between peak incandescence and scattering signals for individual rBC particles measured by the SP2. (b) Scatter plot showing the correlation between the fraction of thickly coated rBC particles (defined as lag time $> 2\,\mu$s) and the MAC at 532 nm.

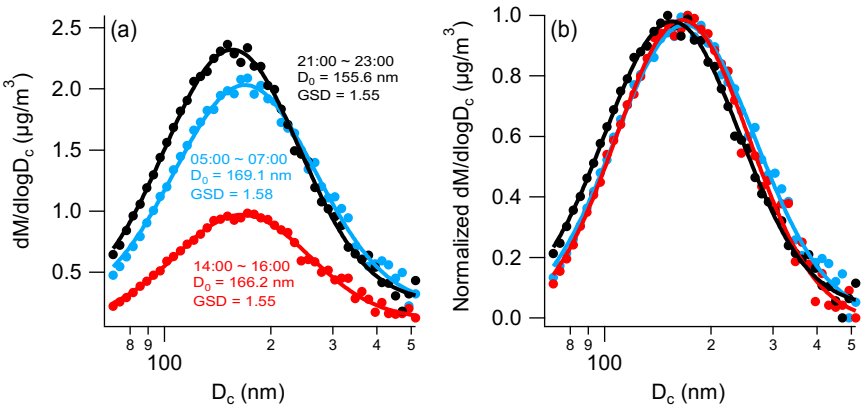

Figure S6. Measured mass size distributions of rBC cores derived from SP2 measurements. Solid lines represent lognormal fits to the observed distributions. Different colors denote different time periods: (a) Absolute mass concentrations. (b) Normalized distributions to facilitate comparison of shifts in MMD and distribution shape across time periods.

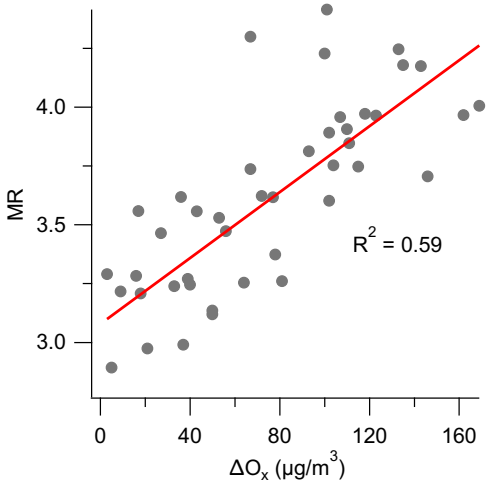

Figure S7. Correlations between MR and ΔO_x.

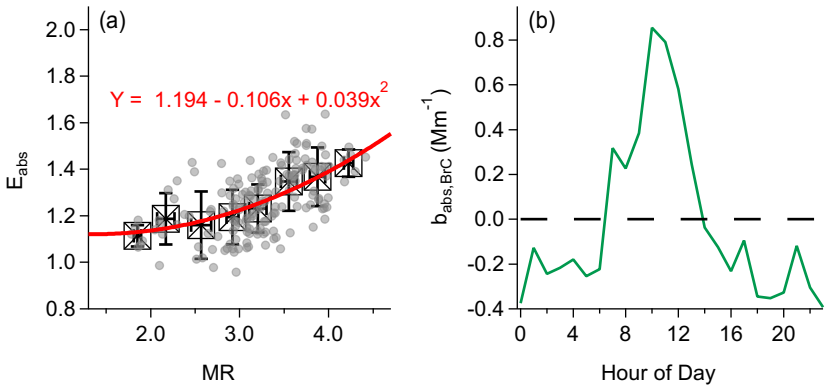

Figure S8. (a) Relationship between E_{abs} and MR at 532 nm. (b) Diurnal variation of brown carbon (BrC) absorption

References

Cappa, C. D., Zhang, X., Russell, L. M., Collier, S., Lee, A. K. Y., Chen, C., Betha, R., Chen, S., Liu, J., Price, D. J., Sanchez, K. J., McMeeking, G. R., Williams, L. R., Onasch, T. B., Worsnop, D. R., Abbatt, J., and Zhang, Q.: Light Absorption by Ambient Black and Brown Carbon and its Dependence on Black Carbon Coating State for Two California, USA, Cities in Winter and Summer, J. Geophys. Res. Atmos., 124, 1550–1577, https://doi.org/10.1029/2018JD029501, 2019.

Healy, R. M., Wang, J. M., Jeong, C.-H., Lee, A. K. Y., Willis, M. D., Jaroudi, E., Zimmerman, N., Hilker, N., Murphy, M., Eckhardt, S., Stohl, A., Abbatt, J. P. D., Wenger, J. C., and Evans, G. J.: Light-absorbing properties of ambient black carbon and brown carbon from fossil fuel and biomass burning sources, J. Geophys. Res. Atmos., 120, 6619–6633, https://doi.org/10.1002/2015JD023382, 2015.

Polissar, A. V., Hopke, P. K., Paatero, P., Malm, W. C., and Sisler, J. F.: Atmospheric aerosol over Alaska: 2. Elemental composition and sources, J. Geophys. Res. Atmos., 103, 19 045–19 057, https://doi.org/https://doi.org/10.1029/98JD01212, 1998.

Reff, A., Eberly, S. I., and Bhave, P. V.: Receptor Modeling of Ambient Particulate Matter Data Using Positive Matrix Factorization: Review of Existing Methods, J. Air Waste Manage. Assoc., 57, 146–154, https://doi.org/10.1080/10473289.2007.10465319, 2007.

Zhai, J., Zhang, Y., Liu, P., Zhang, Y., Zhang, A., Zeng, Y., Cai, B., Zhang, J., Xing, C., Yang, H., Wang, X., Ye, J., Wang, C., Fu, T.-M., Zhu, L., Shen, H., Tao, S., and Yang, X.: Source-dependent optical properties and molecular characteristics of atmospheric brown carbon, Atmos. Chem. Phys., 25, 7959–7972, https://doi.org/10.5194/acp-25-7959-2025, 2025.

Zhang, G., Fu, Y., Peng, X., Sun, W., Shi, Z., Song, W., Hu, W., Chen, D., Lian, X., Li, L., Tang, M., Wang, X., and Bi, X.: Black Carbon Involved Photochemistry Enhances the Formation of Sulfate in the Ambient Atmosphere: Evidence From In Situ Individual Particle Investigation, J. Geophys. Res. Atmos., 126, e2021JD035 226, https://doi.org/10.1029/2021JD035226, 2021.